Particle-Induced Desorption of Kilodalton Molecules Embedded in a Matrix: A Molecular Dynamics Study

Arnaud Delcorte*

PCPM, Universite Catholique de Louvain, 1 Croix du Sud, B1348 Louvain-la-Neuve, Belgium

Barbara J. Garrison

Department of Chemistry, The Pennsylvania State University, 152 Davey Lab, University Park, Pennsylvania 16802

Received: September 25, 2002; In Final Form: December 12, 2002

Inspired by the analytical interest in matrix/analyte systems for static secondary ion mass spectrometry (s-SIMS), we report on classical molecular dynamics simulations of the 500-eV Ar-induced sputtering of samples composed of 2 kDa polystyrene oligomers embedded in a trimethylbenzene matrix. The statistics of the ejected species and the mechanistic analysis of representative trajectories help us understand the main features of molecular desorption for such matrix/analyte samples. Matrix molecules and clusters, but also analyte molecules and matrix/analyte clusters, are observed among the species ejected after 8.5 ps. The average emission depth of sputtered species decreases as a function of their size. The velocity distributions of analyte molecules and matrix/analyte clusters are centered at ∼400 m/s, which is comparable to MALDI observations. In parallel, the average velocity and internal energy of matrix molecules depend on their depth of origin under the surface, the internal versus kinetic energy ratio increasing with emission depth. The fraction of matrix molecules undergoing chemical reactions increases accordingly with depth. From the mechanistic viewpoint, large molecules and clusters are desorbed in a late stage of the interaction, after the energy initially carried by the atomic collision cascade has been transformed into collective vibrational excitations and molecular motions. These theoretical predictions are compared to experimental results, and routes to improve molecular desorption in s-SIMS are explored.

1. Introduction

The theory of organic molecule sputtering has significantly progressed with the development of sophisticated molecular dynamics (MD) simulation codes.[1] On the basis of recent studies involving molecular monolayers on metal substrates[2] and simple bulklike organic samples,[3,4] the elucidation of sputtering processes has become a realistic goal for more complex systems including multicomponent solids. Currently, MD simulations allow us to gain insight into the desorption physics of real-world organic samples either to understand or predict new systems of opportunity for the analytical world.[5]

This theoretical study is part of a multifaceted project investigating novel sample preparation routes in order to improve the performance of static secondary ion mass spectrometry (SIMS) for the analysis of organic samples. The present article focuses on the sputtering mechanisms at play when a bicomponent system, composed of kilodalton analyte molecules embedded in a low molecular weight matrix, is bombarded by kiloelectronvolt particles. The rationale behind the analysis of such systems is the renewed interest in this type of sample preparation procedure in SIMS,[6−12] parallel to the explosion[13,14] of the sister method, matrix-assisted laser desorption ionization (MALDI).[15,16]

The idea of diluting analyte molecules in a solid matrix, however, preceded the invention of MALDI. Michl and co-workers were among the first groups to analyze such samples by SIMS using a frozen rare gas (Ar) as a matrix for small organic molecules.[17] In the original articles by Cooks and co-workers, it is reported that the use of a matrix such as NH_4Cl results in the ejection of ions with a lower internal energy because fewer fragmentation products are observed in the mass spectra.[18−21] The authors proposed that analyte and matrix molecules are sputtered from the surface in the form of clusters. After emission, these clusters cool via evaporation, releasing analyte molecules with low internal energy. Among inorganic materials, Ross and Colton investigated the use of carbon, which is particularly helpful in the analysis of polycyclic aromatic compounds.[22,23] Several authors also perceived the advantages of a liquid matrix,[24,25] a key element at the origin of fast atom bombardment (FAB) mass spectrometry.[26,27] Besides introducing neutral particle beams as an alternative to primary ion beams (SIMS), the developers of the method, Barber and co-workers, popularized the use of glycerol matrices. In comparison with solid matrices, an additional role of the liquid matrix is to refresh the sample by evaporation and/or macroscopic flow under ion beam bombardment.[28] Nevertheless, Gillen et al. also reported enhanced secondary ion signals for small biomolecules embedded in a *frozen* glycerol matrix.[29] In a different spirit, Gillen and co-workers also used gelatin matrices as a model of biological tissues for studying secondary ion emission from embedded tetraalkylammonium salts[30] and biological compounds.[31]

In more recent studies using solid matrices, other authors report an important improvement of the molecular ion emission

* Corresponding author. E-mail: delcorte@pcpm.ucl.ac.be. Phone: 32-10-473582. Fax: 32-10-473452.

10.1021/jp022142g CCC: $25.00
Published on Web 02/15/2003

efficiency for large biological compounds (polypeptides, oligonucleotides) and also for synthetic polymers,[7] with respect to conventional preparation procedures. Wu and Odom compare a series of MALDI matrices and biological analytes with various masses including porcine renin substrate (MW = 1759 Da), human β-endorphin (MW = 3465 Da), bovine insulin (MW = 5733 Da), and bovine ubiquitin (MW = 8565 Da). They find that 2,5-dihydroxybenzoic acid matrices provide the best efficiency for most samples.[6] In parallel, Wittmaack and coworkers measure a very large analyte-to-matrix detection efficiency (i.e., the analyte-to-matrix peak area ratio normalized by the corresponding concentration ratio in solution) for human angiotensin II (MW = 1046 Da), chain B of bovine insulin (MW = 3496 Da), and porcine insulin (MW = 5778 Da) in α-cyano-4-hydroxycinnamic acid using different projectiles including Xe^+ and SF_5^+.[10,32]

From the quoted studies, it is not clear what proportion of the efficiency enhancement provided by the matrix is attributable to the desorption and to the ionization step of the molecular ion emission process.[6,10] As is the case for MALDI, different concepts regarding both the dynamics of desorption and the chemistry of ionization have been proposed to play an important role in the characteristic behavior of matrix/analyte samples. Concerning ionization, Cooks and Busch noticed that selected matrices modify the sample *prior* to sputtering, via the creation of preformed analyte ions.[21,33] Wu et al. emphasize the strong proton donor properties of MALDI matrices, which probably promote the formation of the $(M + H)^+$ ions observed at high intensities in their mass spectra.[6] In contrast with MALDI, though, ionization is not considered by these authors to be the result of a gas-phase process. Concerning desorption, we already mentioned the hypothesis of internal energy reduction accompanying the desolvation of large clusters containing matrix and analyte molecules[21] (also valid for MALDI[34,35]). The clusters themselves are proposed to be sputtered after cooling of the collision cascade in a subsequent stage of the interaction formulated by different authors either in terms of thermal spikes[36] or shock waves[37] (spraying mechanism[38]). Wu et al. also suggest that the nestled environment provided by the matrix ensures a softer emission mechanism.[6] Another effect of the matrix is to separate reactive analyte molecules.[21] Even when reactivity is absent, analyte isolation[39] by the low molecular weight matrix might be important for intact analyte observation.

In this work, we investigate the mechanistic aspects of matrix/analyte sample sputtering (i.e., the desorption stage of the molecular ion emission process). The chosen analyte and matrix are, respectively, styrene oligomers (PS16; 16 repeat units; MW ≅ 2 kDa) and trimethylbenzene molecules (TMB; MW = 120 Da). The choice of pure hydrocarbon molecules is suggested by the available interaction potentials for MD simulations, in particular, the sophisticated AIREBO potential including van der Waals interactions yet allowing molecules to react.[40] We believe that hydrocarbon molecules are appropriate to describe the global dynamics of bombarded matrix/analyte systems. The PS16 oligomer is a good approximation of a polymeric/polypeptide chain, and it has been studied in our previous simulations using silver substrates.[41] The TMB matrix has been chosen for its size, its resemblance to 2,5-dihydroxybenzoic acid (benzene ring with residues), and for the relatively high H content provided by the three methyl radicals, which should favor hydrogen transfer in the bombarded medium.

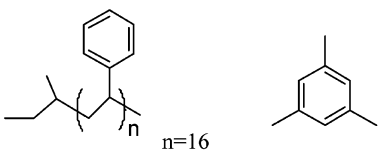

PS16 **TMB**

The validity and power of the present MD model for the study of organic molecule sputtering has been demonstrated in previous works.[1,2] The calculated kinetic energy and angular distributions of benzene molecules sputtered from monolayers adsorbed on silver match the experimental distributions.[42] In the same manner, the energy distributions of fragment and parent ions sputtered from polystyrene oligomers are well described by the model.[43] The narrow polar-angle distribution of vertical, σ-bonded pyridine is also explained by MD simulations.[44] Other studies demonstrated that the MD model correctly predicts the nature of the fragments and clusters sputtered from alkyl[45] and alkanethiol[46] adsorbates. The performance of the AIREBO potential, including long-range forces, has also been verified in recent works, and the nature and kinetic energy distributions of secondary species sputtered from a 7.5-kDa macromolecule have been correctly modeled.[4,47,48]

The results presented in this article explore the dynamics of the desorption process in detail using various trajectory representations to emphasize either the overall action or the specific momentum and energy-transfer processes taking place at different times in the sputtering event. Statistics are collected over a significant number of trajectories to analyze the relative yields of sputtered species, their depth of origin, and their velocity distributions. For comparison, the simulation results are also accompanied by recent experimental measurements using hydrocarbons.[49] In turn, the discussion addresses several of the issues raised in this field over the years, such as the specific influence of the matrix in the desorption process, the question of the yield enhancement/reduction with respect to other systems, the relative importance of interatomic binary collisions and collective motions in the molecular desorption process, the possibility of large cluster emission and their subsequent decomposition, and the issue of chemical reactions (e.g., hydrogen transfer) in the energized organic sample. The relevance of concepts such as "nestled environment" and "matrix isolation" is also investigated. From the mechanistic viewpoint, the big picture emerging from the results is that, beside the emission of surface molecules and fragments directly induced by atomic collision processes, a large fraction of the sputtered material, in particular, the analyte molecule, is desorbed at later times, when the projectile energy is almost randomly distributed among the many bonds of the matrix and analyte molecules. Schematically, the emission of large amounts of organic material is caused by the reaction between the quickly energized volume and the surrounding "cold" medium, inducing the expansion of the surface matrix and analyte molecules in the vacuum. The liberation of the analyte molecule during the emission process is primarily due to the weakness of the van der Waals forces that are unable to maintain the unity of the departing excited volume.

2. Method

The Ar bombardment of *sec*-butyl-terminated polystyrene (PS) oligomers embedded in a trimethylbenzene (TMB) matrix is modeled using molecular dynamics (MD) simulations. The details of the simulation scheme are described elsewhere.[42,43] Briefly, Hamilton's equations of motion are integrated over some time interval to determine the position and velocity of each particle as a function of time.[50,51] The energy and forces in the system are described by many-body interaction potentials. The

TABLE 1: Parameters for the Ag−C and Ag−H Lennard-Jones potential $V = 4\epsilon\left(\left(\frac{\sigma}{r}\right)^{12} - 2\left(\frac{\sigma}{r}\right)^{6}\right)$

	σ (Å)	ϵ (eV)
Ag−C	2.3	0.05
Ag−H	2.3	0.0083

C−C, C−H, and H−H interactions are described by the AIREBO potential. This potential is based on the reactive empirical bond-order (REBO) potential developed by Brenner for hydrocarbon molecules.[52−54] To overcome the limitation of the REBO potential to short-range interactions, the AIREBO potential introduces nonbonding interactions (van der Waals) through an adaptative treatment that conserves the reactivity of the REBO potential.[40] Recently, the AIREBO potential has been used to model the sputtering of solid benzene crystals[3] and polystyrene macromolecules adsorbed on silver surfaces.[4] The Ag−C and Ag−H interactions are described by pairwise additive Lennard-Jones potential functions, with the parameters given in Table 1. The equilibrium distance (σ) has been taken from an estimate for the height of benzene above the Ag{111} surface[55,56] whereas the energy-well depth (ϵ) has been chosen to obtain a reasonable binding energy value for polystyrene molecules ($\sim$2.3 eV) on the same metal surface.[43] To model the Ag−Ag interactions, we used the molecular dynamics/Monte Carlo-corrected effective medium (MD/MC-CEM) potential for fcc metals.[57] The Ar−C, Ar−H, and Ar−Ag interactions are described by purely repulsive Molière potential functions.

For comparison purposes, three different samples have been synthesized in this study. Their characteristics are summarized in Table 2. The first sample is simply constituted by a polystyrene 16-mer deposited on top of a 9-layer silver microcrystallite, much like the samples described in refs 41 and 43. Its purpose in this study is to provide a reference to which desorption of the same molecule in a matrix can be compared. It will be referred to as the "substrate" (S) sample in the manuscript. The two other samples consist of PS 16-mers embedded in a TMB molecule matrix. Top and side views of these two systems after relaxation are shown in Figure 1. These samples have been obtained via a step-by-step procedure alternating analyte/matrix molecule aggregation stages and sample relaxation stages to reach a minimum-energy configuration. The sample in the right part of Figure 1, called the "matrix" (M) sample in the text, is an aggregate of 4 PS 16-mers and 104 TMB molecules. Its shape is that of an ellipsoid with the revolution axis along the *z* direction (i.e., the bombardment direction). The largest diameter of the ellipsoid is 50 Å, and its equatorial diameter is 35 Å. Because of its size and shape, it should be considered more as an organic nanoparticle than a semi-infinite medium with respect to the interaction volume created by an incoming kiloelectronvolt energy projectile. The main reason for limiting the size of this sample is the tractability of the calculations. It will be shown that sample M is large enough to contain the atomic collision cascade induced by 500-eV Ar projectiles but not the subsequent molecular motions that often lead to its disintegration. In addition, the average computation time is still significant with sample M (Table 2), and it prevents running the large number of 10-ps trajectories needed to collect full statistics. For these reasons, a third system has been designed, the "hybrid" (H) sample, which uses a cubic silver microcrystal with a half-spherical cavity on the top as a substrate for the organic molecule blend. In other words, the organic nanoparticle is embedded in the silver crystal. The thickness of the organic sample is 25 Å, and the total size of the system is approximately $50 \times 50 \times 35$ Å^3. As shown in Table 2, this design reduces the computer time for a full trajectory calculation by a factor of 2 on average as compared to that of sample M, allowing us to run a significant number of trajectories in a reasonable amount of time. The effect of the organic sample boundaries on the confinement of the cascade energy will be addressed in detail in the Discussion.

For the bombardment itself, primary Ar atoms are directed along the surface normal with a kinetic energy of 500 eV. Projectile energy and angular distributions, minimal in the experiments, are not considered in the simulations. A representative set of Ar aiming points or trajectories directed within the impact area (white rectangle in Figure 1) are calculated. The aiming points are uniformly distributed in the impact area. A total of 200 trajectories were computed with samples S and M. Four hundred forty trajectories were calculated with sample H. Each trajectory is initiated using a fresh undamaged sample. The initial temperature of the sample is 0 K, and the system is not thermostated during the trajectory calculation.[58] Rather, open boundary conditions are used for the system. That is, energetic particles that reach the sides or bottom of the computational cell are allowed to exit, taking their energy with them. At the end of each trajectory, atoms that have a velocity vector directed away from the surface and are at a height of 8 Å above the top of the sample are considered to be sputtered atoms. For identifying clusters, pairs of atoms are checked to see if there is an attractive interaction between them, in which case they are considered linked.[59,60] A network of linked pairs is constructed, and the total internal energy of the group is evaluated. If the total internal energy is less than zero, then the group of atoms is considered to be an ejected molecule. In some cases, these clusters may have sufficient internal energy to decay unimolecularly during the flight to the detector.[43,60] In all of the considered systems, the mass of hydrogen is taken to be that of tritium (3 amu) to increase the computational efficiency.[42] For a similar reason, that is, to limit computational costs, one configuration has been sampled for each type of system (H, M). The similarity between the mass and velocity distributions obtained with samples H and M shows that the influence of the exact arrangement of the analyte and matrix in the sample is not predominant.

All trajectories are calculated for a minimum duration of 20 ps for sample S, 8.5 ps for sample H, and 4.5 ps for sample M. Certain trajectories for which the number of ejected atoms does not saturate after this first period are restarted with a longer time. At the end of the trajectories, experimentally observable properties such as total yield, yield distribution, kinetic energy, and angular distributions are calculated from the final positions, velocities, and masses of all of the ejected species. Mechanistic

TABLE 2: Characteristics of the Samples and Performed Computations

		number of molecules/atoms				5-ps trajectory hours/node	number of trajectories
size (Å^3)		PS16	TMB	C, H	Ag		
sample S	$35 \times 35 \times 30$	1		270	9×156	1.5	200
sample H	$50 \times 50 \times 35$	2	52	1632	2778	6	440
sample M	$35 \times 35 \times 50$	4	104	3264		12	200

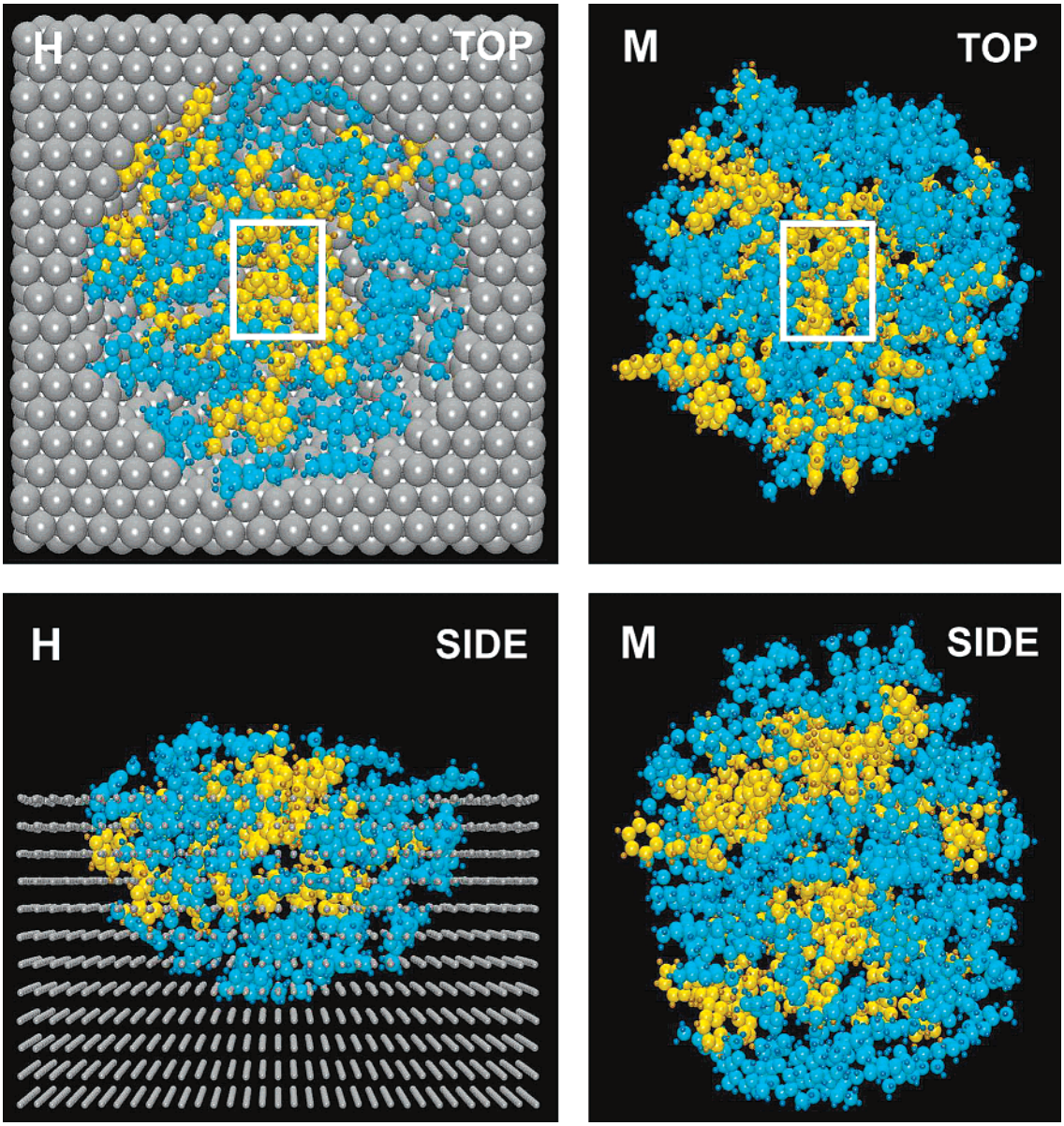

Figure 1. Top and side views of the computational cell of samples H and M. The atoms belonging to the PS16 oligomer are golden, and those of the TMB matrix are turquoise. The silver atoms of sample H are represented by large gray spheres in the top view and, for visualization purpose, by small gray spheres in the side view. The impact area is indicated by a white rectangle in both top views.

information is obtained by monitoring the time evolution of relevant collisional events.

3. Results and Discussion

The goal of this article is to elucidate the physical processes related to the sputtering of bicomponent organic samples composed of long oligomer chains embedded in a low molecular weight molecule matrix. In section 3.1, we compare the calculations performed for samples H and M and evaluate their specific merits for modeling real samples, which are semi-infinite with respect to the size of the interaction volume. We show that sample H constitutes a tractable and adequate model considering the scope of this study. In section 3.2, the yields, depth of origin, and velocity distributions of sputtered species are analyzed in detail, providing us with statistically significant information that helps in completing the mechanistic picture envisioned in section 3.1. Chemical reactions (hydrogen transfer) are also investigated. The link to relevant experimental results is made in section 3.3, and analytical perspectives are proposed in the Conclusions.

3.1. Comparison of the Samples. 3.1.1. Time Evolution of the Sputtering Process. Characteristic trajectories involving samples H and M are depicted in Figures 2 and 3, respectively. Both events show the emission of an entire PS16 oligomer together with a large number of TMB molecules and some fragments at a time between 5 and 10 ps after the projectile's impact on the sample surface. In both cases, the second PS16 molecule embedded in the matrix breaks apart as a result of the interaction with the primary particle and/or with recoil atoms of the collision cascade. The whole organic nanoparticle starts disintegrating after a few picoseconds in both events. Such an extensive decomposition has rarely been observed in our first study involving a large PS molecule comprising 61 styrene repeat units, mostly because it was held together by strong covalent C−C bonds and not by much weaker van der Waals interactions. A similar phenomenon was also noticed by Krantzman and co-workers for solid benzene crystals bombarded by 300-eV Xe projectiles.[3] On a smaller scale, it is also reminiscent of the processes observed when modeling the

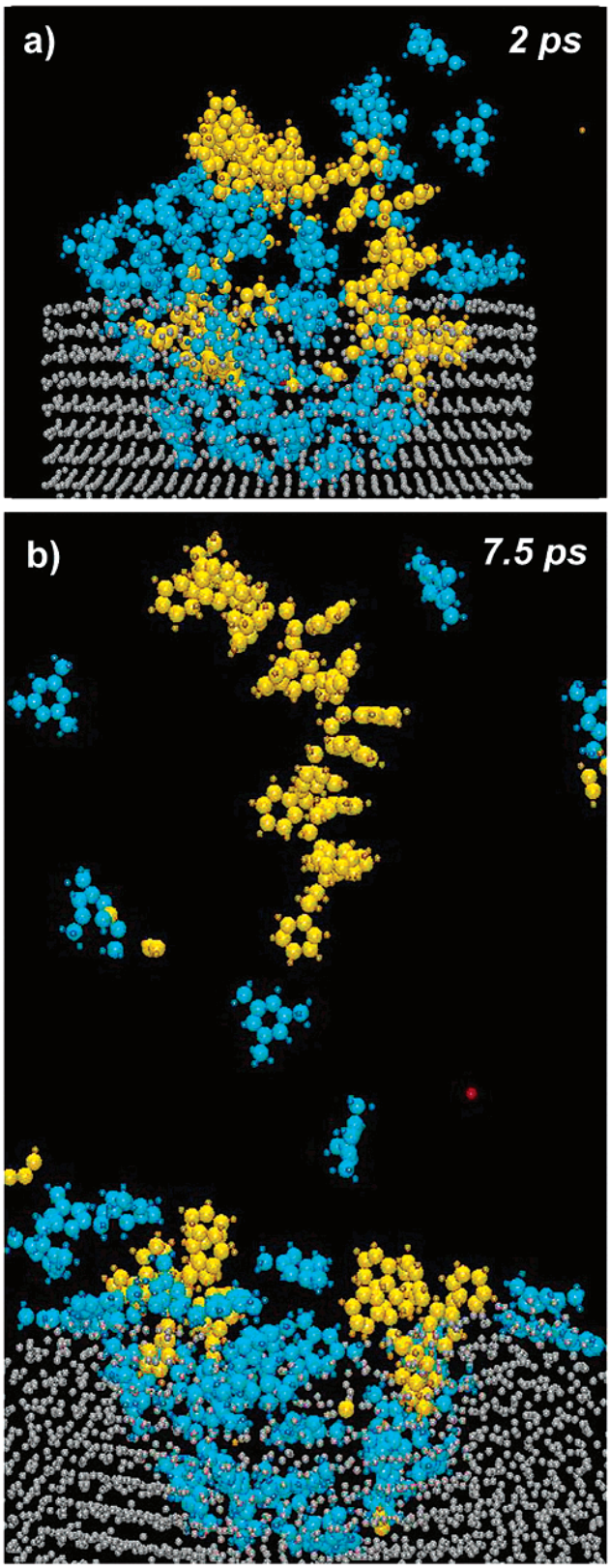

Figure 2. Sputtering sample H. Snapshots of the time evolution of a characteristic trajectory showing the ejection of the entire PS16 oligomer along with TMB molecules and fragments (a) after 2 ps and (b) after 7.5 ps. Note the recombined TMB molecule (left side) including a C atom from the fragmented PS16 molecule.

interaction of a laser beam with molecular nanoparticles[61] and with oligomers embedded in matrix.[62]

At this point, there is already a noticeable difference between the sputtering of samples H and M. In sample H, the action is

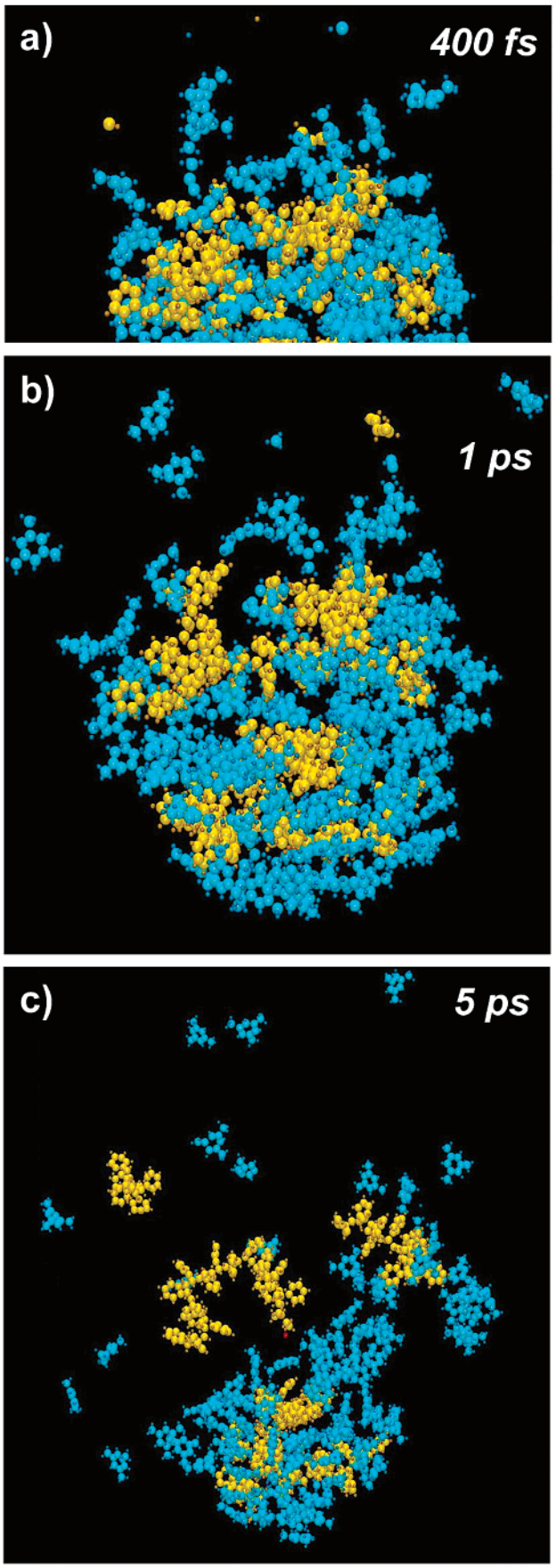

Figure 3. Sputtering sample M. Snapshots of the time evolution of a characteristic trajectory showing the ejection of the entire PS16 oligomer, accompanied by TMB molecules and clusters, and the decomposition of the organic sample (a) after 400 fs, (b) after 1 ps, and (c) after 5 ps.

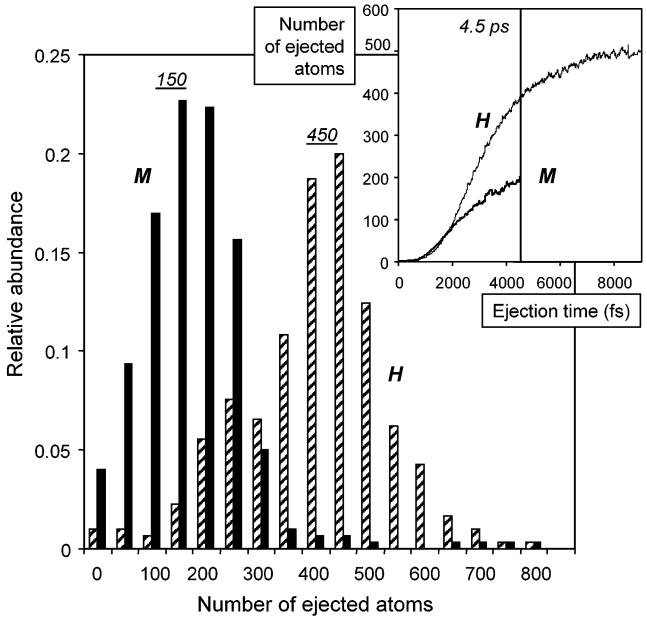

Figure 4. Distributions of the number of ejected atoms at 4.5 ps for samples M (solid bars) and H (hatched bars). Inset: time evolution of the average number of sputtered atoms (forward-moving average over 100 bins) for the full set of trajectories (sample H, thin line; sample M, thick line).

confined by the surrounding silver crystal (small gray spheres), which seems to refocus the momentum upward without a dramatic alteration of the silver medium itself, much like heated corn popping up from a pot (a comparison that has already been used by several authors in the field of organic sample sputtering[63] and laser ablation[64]). In sample M, the projectile momentum, randomized in the entire organic sample via the collision cascade and subsequent molecular motions, is not preferentially redirected upward because of the absence of a metallic medium. The large amount of energy transferred to the organic nanoparticle eventually causes its decomposition, with molecules and clusters being ejected in various directions. The influence of the organic sample boundaries regarding the amount of ejected material and its mechanistic explanation are examined more closely in the following subsections.

3.1.2. Number of Sputtered Atoms. To compare the amount of material sputtered with samples H and M, we monitor the time evolution of the numbers of sputtered atoms and calculate their distribution for the full collection of trajectories. The main frame of Figure 4 shows the distributions of the number of sputtered atoms collected over 440 trajectories for sample H and 200 trajectories for sample M, 4.5 ps after projectile impact. The chosen time (4.5 ps) corresponds to the minimum trajectory duration for sample M, as explained in the Method section. In addition to the distributions at a given time, the inset of Figure 4 indicates the time-dependent average of the number of ejected atoms for the two series of trajectories (black lines). The numbers of atoms discussed in this section include all of the ejected atoms without distinction, whether they are part of a fragment, a molecule, or isolated particles. The abundance of ejected species is discussed in relation to their mass and chemical structure in section 3.2.1.

The amount of emission caused by the projectile ranges from 0 to about 800 atoms per trajectory. At 4.5 ps, the distributions peak at 150−200 atoms for sample H and at 400−450 atoms for sample M, and their shapes below the maximum differ significantly. These broad distributions indicate that there is a relatively wide range of sputtering characteristics, going from almost no emission to the emission of about 50% of the embedded organic matter for sample H and 25% of the whole nanoparticle for sample M. The average curves (inset) match closely before 1.5 ps, but they start diverging significantly afterward. After 8.5 ps, the average curve corresponding to sample H saturates for a value of 500 sputtered atoms. In comparison, the extrapolation of the average curve up to 8.5 ps indicates a value in the range of 200−250 atoms for sample M. The mechanistic reason for this divergence, which is related to the effect of the silver substrate in sample H, is explored hereafter. In practice, the results show that confining the organic sample significantly increases the sputtering yield.

3.1.3. Mechanistic Interpretation. The results of a mechanistic analysis of high sputtering yield events are illustrated by the case study of the two trajectories already introduced via the movie snapshots of Figures 2 and 3. To probe the physics of the first stages of the sputtering process, comprising the momentum transfer from the projectile to the target atoms and the subsequent atomic and molecular motions in the sample, we use collision trees[41] and snapshots of the trajectories showing the energy and momentum of the atoms (energy movies).[43] The collision trees show the branching of the atomic collision cascades over the first 100 fs of the trajectories via the simultaneous representation of the successive atomic positions in a single viewgraph. The atoms are colored if they are set in motion by a collision transferring more than 10 eV of kinetic energy, and they are turned off when their kinetic energy drops below 5 eV.[4] In the energy movies, the diameters of the atoms are proportional to their kinetic energy up to 5 eV. In comparison with the collision trees, the energy movies also show the low-energy part of the interaction, when atoms have insufficient energies to break covalent bonds (<5 eV), which usually corresponds to longer times in the chronology of the events.

The collision trees and energy movies of the trajectories are shown in Figure 5 (sample H, trajectory of Figure 2) and Figure 6 (sample M, trajectory of Figure 3). In the trajectory depicted in Figure 5 (Figure 2), the projectile collides with a few atoms at different stages of its path in the organic sample, finally creating a denser network of subcascades near the matrix−metal interface (Figure 5a). The cascade density is mirrored by the first snapshot of the energy movie (Figure 5b, 61 fs), where many atoms are moving downward with more than 5 eV of kinetic energy. In the second snapshot of the energy movie (Figure 5c, 233 fs), the collision cascade is over, as indicated by the low kinetic energy of the moving atoms (<3 eV).[4] There are two important features depicted in Figure 5c. First, even though the atomic/molecular motions in the organic sample have reached the silver medium, there is almost no motion of the silver atoms. Second, in comparison with the situation at 61 fs, the direction of the motion has been essentially reversed, from downward (blue balls) to upward (red to yellow balls). The silver container acts like a wall with respect to the moving organic sample, reflecting a large fraction of the momentum and energy outward. This upward motion is followed at later times by the ejection of a large amount of organic material (Figure 2).

In the trajectory depicted in Figure 6 (sample M, Figure 3), the projectile induces a dense cascade in the top part of the organic medium before penetrating deeper into the sample. The energy movie snapshot of Figure 6b shows that the atomic cascade is still unfolding after 48 fs, with many atoms being set in motion by the projectile in a manner that is qualitatively similar to that observed for sample H in Figure 5b. After 172 fs (Figure 6c), however, the situation has changed with respect to sample H. Even though part of the momentum is reflected

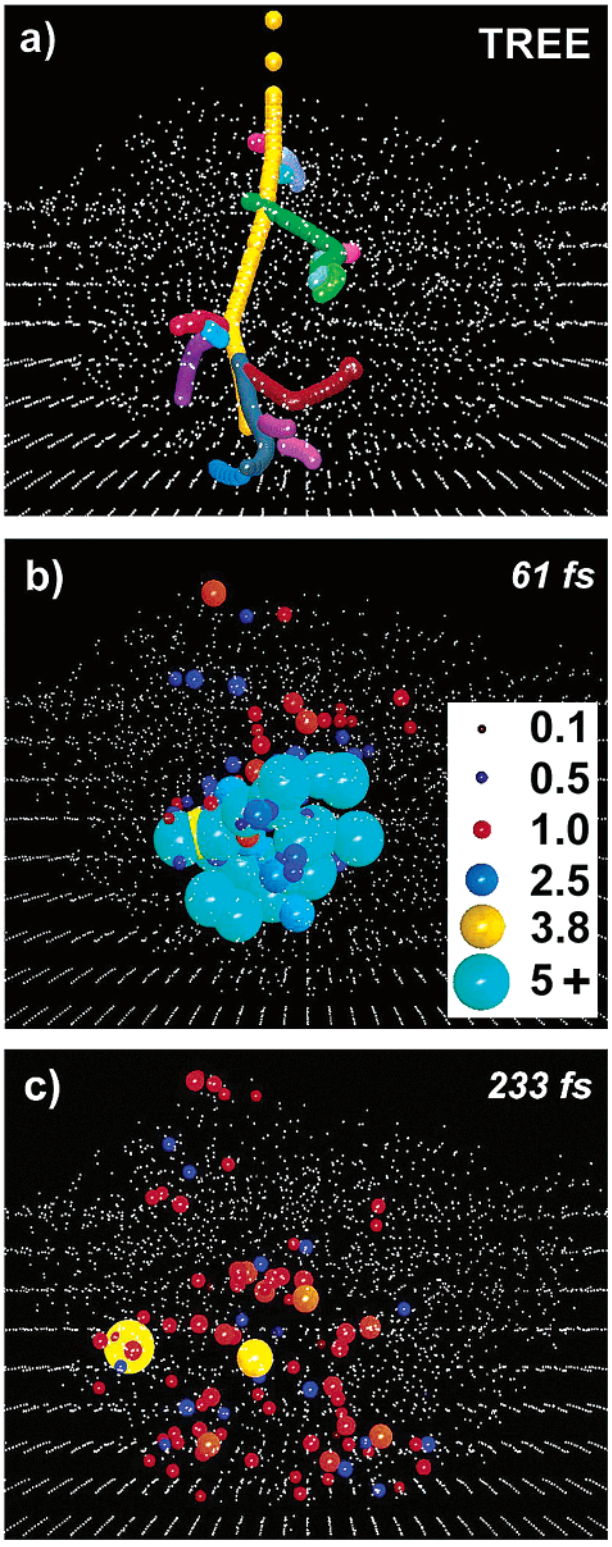

Figure 5. Mechanistic analysis of a representative trajectory for sample H. (a) Collision tree. The successive positions of atoms in the collision cascade are represented by colored spheres. The Ar projectile is bright yellow. (b−c) Energy movie snapshots. The size and color of the spheres are coded as a function of kinetic energy and momentum. Small blue to large turquoise (respectively, small red to large yellow) spheres correspond to downward- (respectively, upward) moving atoms of increasing kinetic energy. Atoms at rest are represented by white dots. (b) 61 fs. (c) 233 fs.

toward the surface, as indicated by the large number of red to yellow balls in the top part of the sample, there is still a large number of atoms moving downward deep in the sample, as

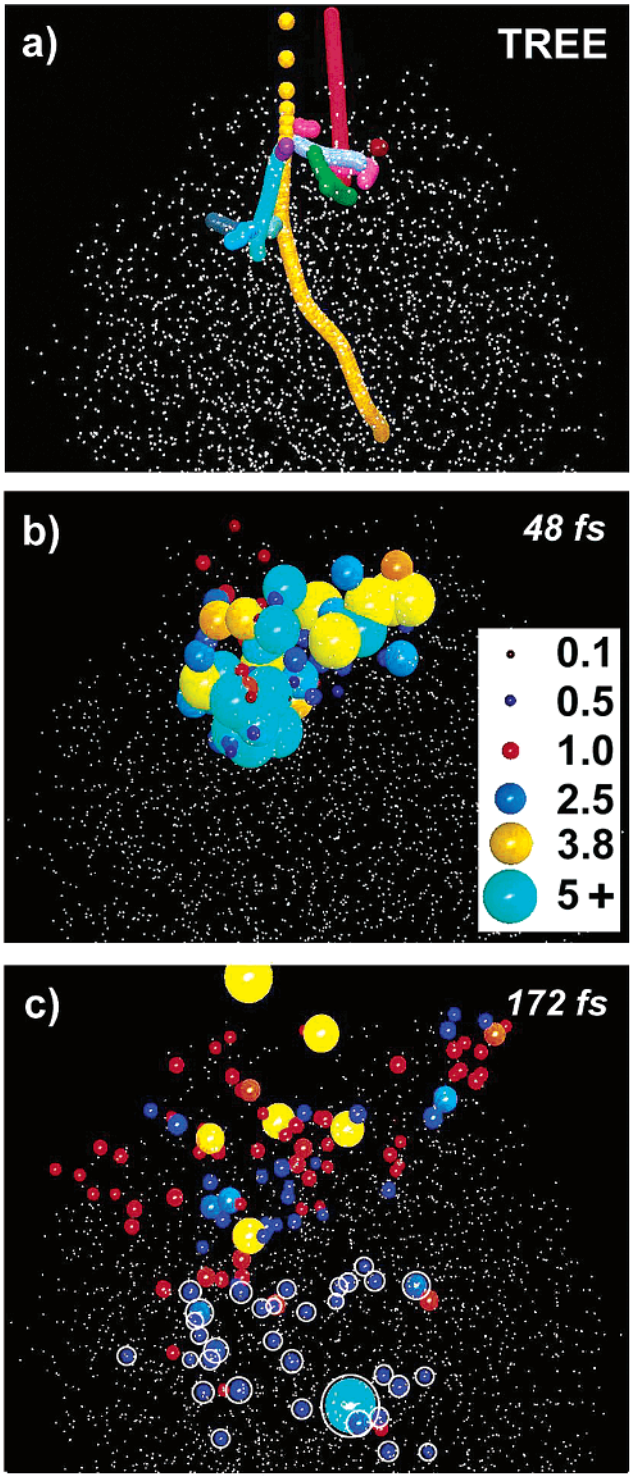

Figure 6. Mechanistic analysis of a representative trajectory for sample M. (a) Collision tree. (b−c) Energy movie snapshots: (b) 48 fs; (c) 172 fs. (See the text for details.)

indicated by blue balls marked with white circles. This expanding population of moving/vibrating atoms eventually induces molecular emission and sample disintegration.The analysis of the dynamics shows that the momentum is not as efficiently redirected toward the surface in sample M as in sample H. The enhanced reflection caused by the presence of a metal substrate explains the higher yield of ejected species measured for sample H (Figure 4). In addition, because of the spherical shape of the silver container, the molecules and fragments moving sideways

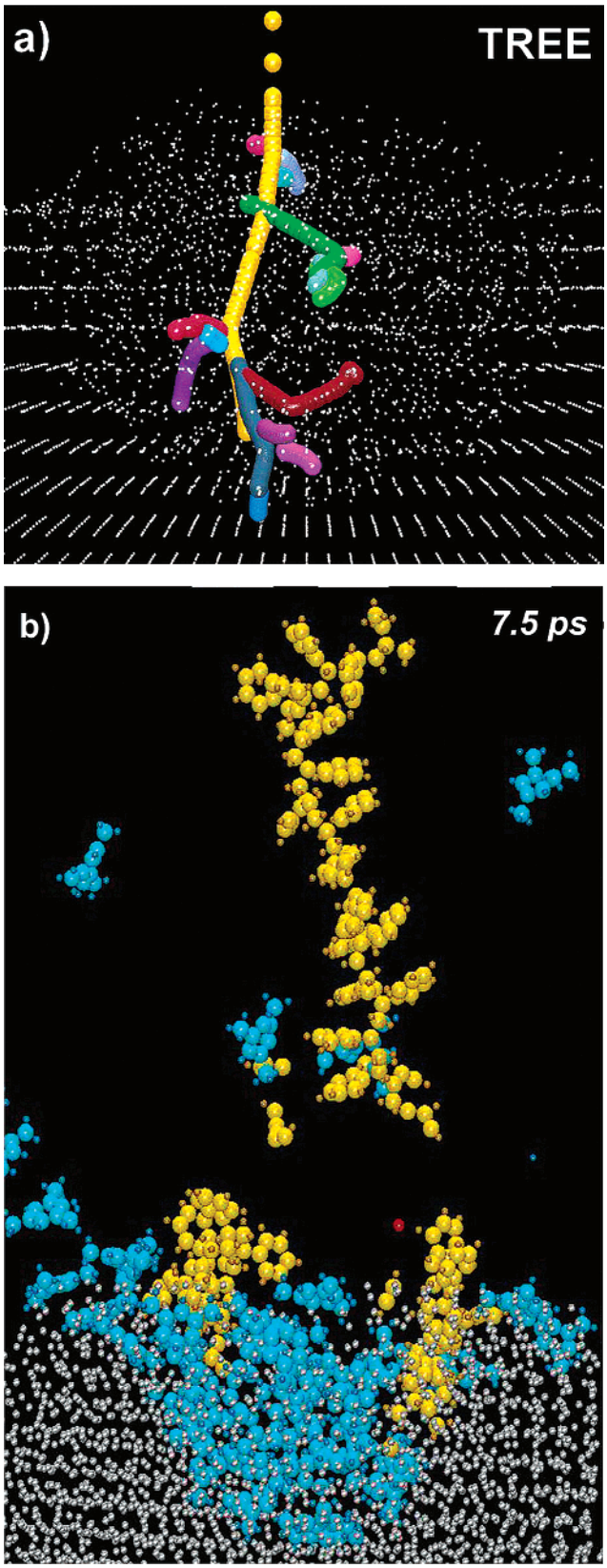

Figure 7. Mechanistic analysis of a trajectory calculated with the same aiming point as that described in Figure 5 but with Ag atom masses reduced to 12 Da. (a) Collision tree. (b) Snapshot of the trajectory movie (7.5 ps).

are also redirected upward in sample H whereas they can leave the solid and not be counted as yield in sample M.

To check the influence of the substrate atom mass on the energy reflection mechanism, we reran a series of trajectories with ^{12}Ag instead of ^{108}Ag. The trajectory with the same projectile aiming point as in Figure 2 is shown in Figure 7. First, the collision tree is almost exactly the same with ^{12}Ag (Figure 7a) as with ^{108}Ag (Figure 5a) because most of the action unfolds in the organic sample before any effect from the surrounding medium might be sensed. The trajectory of the last two recoil atoms (gray and blue, bottom of the tree), however, is significantly influenced by the isotopic change. In Figure 5a, the gray atom is obviously deflected by the ^{108}Ag interface so that it collides afterward on the left of its initial trajectory, transferring this lateral component of momentum to the blue atom. In Figure 7a, the gray atom keeps its trajectory and collides with another atom that implants deeper into the ^{12}Ag crystal. In addition, the movie snapshot of the situation after 7.5 ps (Figure 7b) indicates that the two trajectories are almost equivalent in terms of sputtered species, regardless of the mass of the silver isotopes.

Our analysis shows that the mechanism of momentum reflection does not correspond to the cases described in the literature for overlayers of small organic molecules adsorbed on heavy-metal substrates.[65,66] In a situation where the energy of the moving atoms is high (collision cascade) and their interactions can be considered to be elastic collisions, the maximum quantity of energy and the momentum transferred per collision are governed by the masses of the involved atoms rather than the lattice structure and bond strengths. This situation is the case described by Taylor and Garrison.[66] Here, the momentum reflection is independent of the substrate atom mass and, in the dynamics, it is not related to the atomic collision cascade development. As indicated by the energy movies, the momentum reflection is part of the molecular motion stage of the interaction. In sample H, the energy is very poorly transferred to the substrate because the high-frequency vibrations of the organic molecule are mismatched with the low-frequency phonon modes of the Ag solid. Therefore, the momentum is almost entirely reflected toward the surface. This interpretation is confirmed by the different behavior observed for sample M, where energy can diffuse better in the sample through the network of equivalent bonds.

With respect to the average sputtering yield described in Figure 4, our samples are two extreme cases, and semi-infinite matrix/analyte samples such as those probed by kiloelectronvolt ions in experimental devices should fall between samples H and M. Indeed, the metal substrate in sample H clearly enhances the sputtering yield whereas the absence of surrounding inorganic material in sample M certainly reduces the momentum reflection and the yield with respect to a semi-infinite medium. Beside these differences, the processes of collision cascade, molecular motion, and sputtering are qualitatively similar in the two studied systems, as is further confirmed by the velocity distributions described below. Because of this general resemblance, we are confident that the big picture concerning matrix/analyte systems can be deduced from the analysis of the sputtered species in a specific case. Therefore, in section 3.2, we focus on the case study of sample H, which is more tractable than sample M from a computational viewpoint.

3.2. Statistics of the Sputtered Species. 3.2.1. Abundance of Ejected Species. The fragment, molecule, and cluster yields after 8.5 ps are summarized in Figure 8 for sample H. The low-mass range of the mass distribution (Figure 8a) is dominated by small fragments such as C, CH_3, and C_2H_2, as previously observed in the MD simulations of hydrocarbon layers. Other important and more characteristic fragments are C_6H_5 and C_8H_9. A careful analysis of the present results confirms that C_2H_2 and C_6H_5 mostly originate from the PS16 oligomers whereas C

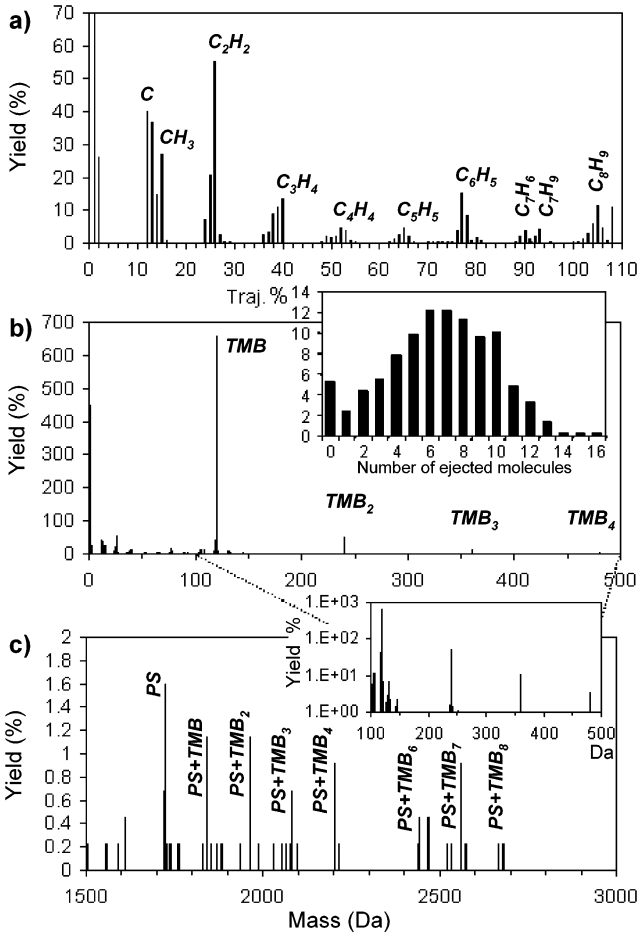

Figure 8. (a−c) Yields of fragments, molecules, and clusters sputtered from sample H after 8.5 ps (440 computed trajectories). Inset of b: frequency distribution of ejected TMB molecules. Inset of c: yields of TMB molecules and clusters on a logarithmic scale.

atoms are almost equally sputtered from the PS16 molecules and from the TMB matrix. In contrast, CH_3 and C_8H_9 are new intense peaks that were weak or absent in our previous simulations. They both result from the fragmentation of the TMB molecule via the loss of a methyl group.

The second frame of Figure 8 shows the mass range of 0−500 Da, including the TMB molecule and clusters containing up to four molecules. The molecular peak is much more intense than any of the fragments described above, and the yield of TMB dimers is comparable to that of the C_2H_2 fragments. Another characteristic of the TMB clusters is that their intensity decreases almost exponentially with mass (inset of Figure 8c). The inset of the second frame (Figure 8b) shows the distribution of events as a function of the number of ejected TMB molecules per trajectory. Except for the local maximum where no molecular ejection occurs, the distribution is symmetric, with a maximum corresponding to the ejection of six to eight TMB molecules, which provides a good indication of the average action observed for such sample and bombardment conditions.

In the high-mass range of the distribution (Figure 8c), there is another series of equally spaced peaks that correspond to clusters including the entire PS16 oligomer and a number of TMB molecules ranging from one to eight. We continued the simulation for these PS16/TMB_x clusters over an extended time of 100 ps. All of them decompose by ejecting TMB molecules in the first 50 ps of the simulations and thus would not be observed in a SIMS mass spectrum that is measured after tens to hundreds of microseconds.

TABLE 3: Comparison of the Sputtering Yields (%) after 8.5 ps for Samples H[a] and S[b]

sputtered species	sample H	sample S
H	162	448
C	40	67
C_2H_2	55	30
C_6H_5	15	5.0
TMB	657	n/a
Ag	11	139
PS16	1.6	4.5
PS16-H + PS16 + PS16/TMB_x	8.7	5.0

[a] PS16 embedded in a matrix. [b] PS16 on a substrate.

The absolute yields of sputtered species have been compared with those obtained with sample S (i.e., a sample where the PS16 molecule is directly deposited on top of a flat silver crystal). The yields after 8.5 ps are summarized in Table 3 for both samples. The longer trajectory time (20 ps) computed for sample S demonstrates that even the molecular yield has reached saturation after 8.5 ps. It appears that the yield of atomic and small fragments is proportionally larger when PS16 is directly deposited on a metal substrate (sample S), whereas larger fragments such as phenyl rings are favored with sample H. For instance, the ratio $Y(C_6H_5)/Y(C)$ is equal to 0.38 for sample H and 0.07 for sample S, which suggests that fragmentation might be more extensive when organic samples are deposited as submonolayers on metal substrates. However, the two last lines of Table 3 indicate that the yields of PS16 molecules are in the same range for both samples. Therefore, embedding large analyte molecules in a low molecular weight organic matrix is as efficient as casting molecules on a metal substrate. In other words, there is not a strict physical limitation preventing the desorption of kilodalton molecules from an organic medium.

3.2.2. Emission Depth of Fragments and Molecules. Figure 9a shows the normalized yield of C and H atoms as a function of their depth of origin in the sample. The yield coordinate represents the convolution of the signal originating from ±1 Å around the exact depth defined in the *x* axis of the graph. To get rid of the influence of the variable atom numbers with depth (geometrical effect), the number of sputtered C (H) atoms is divided by the number of C (H) atoms in the corresponding 2-Å-thick slab of material. The yield of C atoms decays rather steeply, being reduced to 20% of its maximum value between 10 and 15 Å under the surface. In contrast, the yield of H atoms decreases slowly, down to 50% of its initial value at the bottom of the 25-Å organic sample. From an analytical perspective, this result indicates that C atoms are significantly more surface-sensitive than H atoms. This is probably because of the very small size of H atoms, which can travel longer distances in the open organic medium. A comparable difference in behavior between C and H atoms has also been observed by Beardmore and Smith for a crystalline polyethylene sample.[67] In their case, though, both yields level off beyond 20 Å, which might be due to the different bombardment conditions (1-keV Ar; 60° off normal), the sample specifics, or the lack of long-ranged interactions in the simulation.

The emission depth distributions of matrix-related species, namely, CH_3 fragments and the TMB molecule itself, are shown in Figure 9b. For polyatomic particles such as these, the yield has not been normalized because a reasonable determination of the number of potential fragments including rearrangement channels per unit of depth is impossible. The ejection depth of entire TMB molecules is limited to the top 15 Å of the surface. The two-peak structure in the TMB curve is caused by the nanostructure of the sample. The depletion between the two

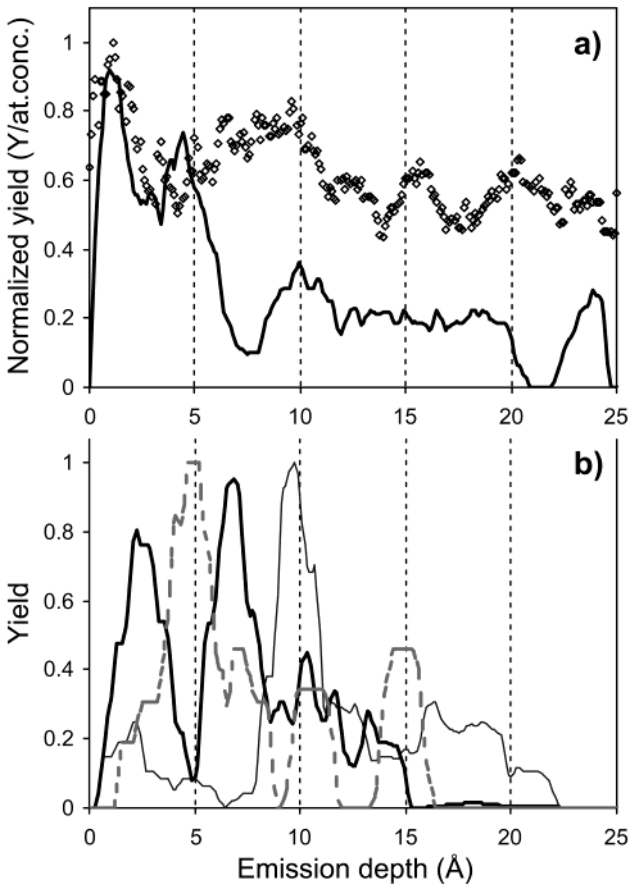

Figure 9. Origin depth distribution of atoms, fragments, and molecules sputtered from sample H. (a) C (—) and H atoms (◊). The yields are normalized by the number of C (H) atoms present in the corresponding slab of material. (b) TMB molecules (**—**), CH_3 fragments (−), and C_6H_5 fragments (- -).

peaks at a depth of 5 Å corresponds to the space occupied by the top PS16 molecule. The second PS16 molecule is localized at about 15 Å below the surface. TMB molecules buried under the second molecule (i.e., between 15 and 25 Å) do not give rise to a significant fraction of the molecular yield. The profile of the CH_3 fragments, also related to the TMB molecules, is completely different. Very few methyl fragments are produced in the top layer, where the entire molecule signal is high, but instead, there is a large peak at 10 Å, where the TMB molecule signal is already strongly reduced. The CH_3 signal decays afterward and levels off at a depth of 22 Å. This result indicates that methyl fragments are preferentially generated at some depth below the surface (peak at 10 Å) and that they can travel from farther away underneath the surface before being emitted. The reason that fragments are mainly produced at some distance from the surface is related to the statistical distribution of bond scissions in the sample. The profile of fragments sputtered from the PS16 molecule, such as C_6H_5 (Figure 9b) and C_2H_2 (not shown), essentially mirrors the specific nanostructure of the sample. In the C_6H_5 profile, two peaks can be noticed at 5 and 15 Å (i.e., where the PS16 molecules are located and the matrix molecule signals are depleted). The relative areas of the peaks are also influenced by the attenuation of the signal for the two different depths of origin corresponding to the separated PS16 molecules. In a similar manner, the PS16 molecule that is buried under 15 Å of organic material is never observed as an intact sputtered species in our simulations.

3.2.3. Velocity Distributions. The velocity distributions of fragments, molecules, and clusters are represented in Figure 10a.

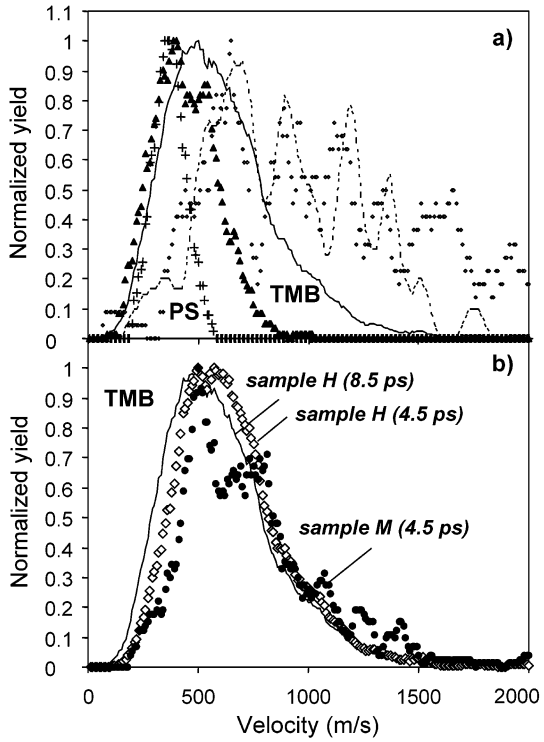

Figure 10. Velocity distributions of organic species. (a) Species desorbed from sample H after 8.5 ps: PS16/TMB_x [$0 \le x \le 8$] (+), TMB dimers (▲), TMB molecules (—), C_6H_5 (- -), C_2H_2 (•). (b) Velocity distribution of TMB molecules emitted from samples H (◊) and M (●) after 4.5 ps. The solid line shows the distribution of TMB molecules after 8.5 ps as a reference.

The velocity spectra of C_2H_2 and C_6H_5 fragments are comparable, except beyond 1500 m/s, where the C_2H_2 intensity is sustained whereas the C_6H_5 intensity quickly drops to zero. In comparison, the velocity distributions of molecules and clusters (TMB, TMB dimers, PS16, and PS16/TMB_x clusters) are narrower, and they peak at a lower velocity. In particular, the fragment velocity spectra are depleted in the range of 0−500 m/s, where the maxima of entire molecules and cluster distributions are found. The slopes of the increasing parts of the distributions up to the maxima, around 500 m/s, are almost identical for TMB molecules, TMB dimers, and PS16/TMB_x clusters. In contrast, the slope after the maximum becomes steeper with increasing particle size. Therefore, besides a fast fraction that decreases with increasing particle size, there is a significant fraction of single TMB molecules and TMB clusters that are ejected with the same velocity as that of much larger entities such as PS16/TMB_x clusters. This observation can be understood by considering the ejection scenario described in Figure 2. Although fast fragments and TMB molecules sputtered in the first picosecond of the interaction have already left the frame in Figure 2a, there is a relatively important number of TMB molecules accompanying the departing PS16 oligomer in a collective upward motion. After 7.5 ps, the PS16 oligomer and several of these TMB molecules hover at a similar distance from the surface, indicating that their velocities are comparable. This scenario is characteristic of an important fraction of the computed trajectories. In comparison with the sputtering of submonolayers of molecules adsorbed on a metal,[41−43] the center-of-mass velocities of the ejected molecules are significantly lower with thick organic solids such as samples H and M.

In section 3.1, arguments based on the mechanistic study of a few representative trajectories have been formulated to support

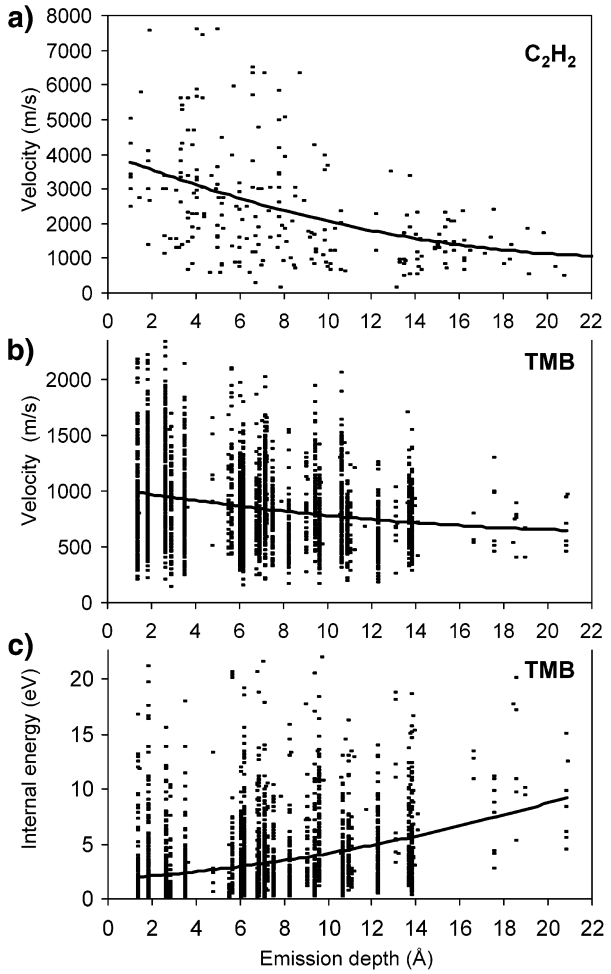

Figure 11. Center-of-mass velocity and internal energy as a function of the depth of origin. (a) C_2H_2 velocity. (b) TMB molecule velocity. (c) TMB molecule internal energy.

the assumption that, even though the sputtering yields were different, the ejection processes were qualitatively similar for samples H and M. This hypothesis can be further validated by comparing the velocity spectra of molecules sputtered from both samples. Figure 10b shows the velocity distributions of TMB molecules ejected from samples H and M over the same period of time, from 0 to 4.5 ps. Because saturation of the MD molecular yield is not reached after 4.5 ps, the spectrum measured at that time is slightly shifted toward higher velocities with respect to the full spectrum at 8.5 ps (sample H). The two velocity spectra measured at 4.5 ps match satisfactorily, despite small differences that are probably due to the lower statistics or to the specific structure of the sample. Therefore, our working hypothesis is validated.

The velocity of each individual ejected C_2H_2 and TMB molecule is shown as a function of the depth of origin in Figure 11a and b with lines indicating the average value. In general, the distributions are very broad although there is a trend of decreasing average velocity for particles originating deeper in the material. The internal energy of individual TMB molecules is shown in Figure 11c. Again, there is considerable scatter in the values as a function of depth but a trend of increasing internal energy for particles originating deeper in the solid. The combination of Figure 11b and c tends to show that the velocity vectors of atoms belonging to the TMB molecules exhibit a higher degree of correlation when they are sputtered from the top rather than from the bottom of the sample. Molecules lying on top of the sample, when they receive upward momentum, can relatively easily free themselves from the surface. In contrast, molecules embedded in the bulk of the sample interact extensively with the surrounding medium before being ejected as separated entities, which favors the randomization of atomic motions. Because of their higher internal energy, these molecules should be more prone to metastable decay than molecules initially sitting in the extreme surface region.

The velocity distributions of matrix and analyte molecules can be compared to those calculated for the MALDI process using molecular-scale MD simulations.[34,35,62,68] Velocity distributions for matrix and analyte molecules have been reported in refs 35 and 68. The profile of axial velocities observed for both matrix and analyte molecules is symmetric, with a maximum around 400 m/s. Although the maximum is close to that observed in our simulations for analyte molecules and cluster species (Figure 10), the laser desorption results mainly indicate that matrix and analyte molecules are entrained together with similar velocities in the ejected plume. There is, however, a slight differential effect of the surface on the velocities of matrix and analyte molecules.[68,69] In the sputtering case, matrix molecules that are initially located in the bulk of the sample are also often entrained with a speed that is similar to that of larger clusters and analyte molecules, but a comparatively more important fraction of the matrix molecules are ejected with larger velocities from the surface region (Figure 10a). Ultimately, it appears that the major phenomenological difference between the sputtering and laser desorption results could be due to the much smaller interaction volume of the sputtering process, which promotes the influence of the extreme surface. In both methods, the energy transferred to the subsurface layers, either by photon absorption (MALDI) or via the collision cascade (SIMS), is quickly transformed into collective motions that are partly correlated (molecular motion) and partly uncorrelated (vibrational excitations). This transformation of different excitations into a similar form of molecular motion is reminiscent of the concept of energy isomerization developed by Cooks a few decades ago,[21,33] and it might explain the similar nature of the desorbed species.

3.2.4. Chemical Reactions. This subsection focuses on the reactions occurring in the organic solid during the bombardment or the emission stage of the sputtering process. It is important to notice that only reactions involving radicals are observable in the MD simulations. Ion/molecule reactions, which constitute a significant part of the chemistry induced by fast projectiles in organic solids,[21,36,70,71] are not taken into account at this stage because ionization pathways are not implemented in the current framework of the model. Even though ions are absent, the possibility of intermolecular reactions (e.g., H transfer) is particularly intriguing because they mimic ion/molecule reactions that constitute important ionization mechanisms in MALDI and SIMS. For instance, hydrogen capture reactions occurring in the MD model have been used in a previous paper to explain the intense C_7H_7 fragment observed in polystyrene SIMS spectra.[43]

In the mass distribution of Figure 8, most peaks are readily attributable to either PS16 or TMB molecules. Products resulting from gross recombination reactions are almost absent from the sputtered material. As was the case for other samples,[1,43,72] though, H abstraction and H exchange reactions are observed. One example is C_6H_6, which is not present as such in any of the molecules before sputtering. In our simulations, 95% of the sputtered benzene molecules are formed via hydrogen capture by a free phenyl initially belonging to one of the PS16

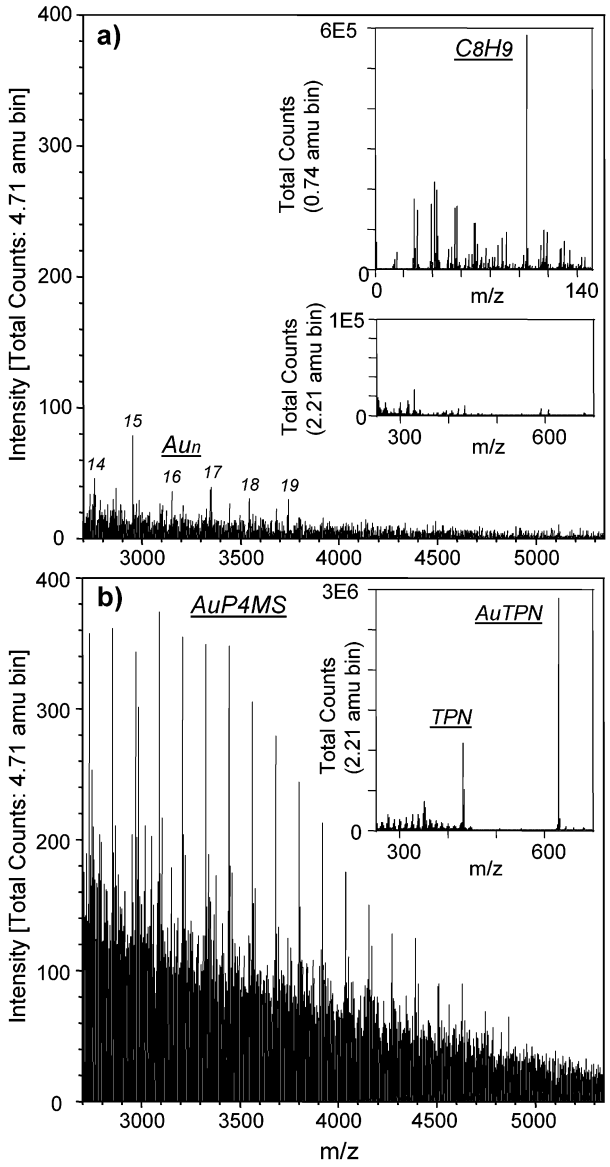

Figure 12. Positive time-of flight secondary ion mass spectra obtained under 12-keV Ga^+ ion bombardment for (a) a Au-metallized poly(4-methylstyrene) sample and (b) a Au-metallized tetraphenylnaphthalene/poly(4-methylstyrene) blend. Both samples are cast from solution on silicon wafers. (See the text for details.)

oligomers. One-sixth of the hydrogen transfer reactions leading to the formation of C_6H_6 is intermolecular.

Investigating a possible relationship between H transfer reactions and the emission depth of the recombining species, we measured the fraction of TMB molecules undergoing H exchange as a function of the *z* coordinate of the molecule's center of mass before emission. This fraction is essentially lower than 1% in the top 5 Å of the sample, between 1 and 10% for the slice of material between 5 and 15 Å, and larger than 10% deeper in the bulk. This observation indicates that chemical reactions (H transfer) are favored in the bulk of the sample and not at the surface. It is consistent with the higher internal energies calculated in Figure 11 for bulk molecules and with the longer time spent by radicals near other molecules for species deeper in the bulk. Even though our conclusions concern the radical/molecule reactions observed in the simulations, it is reasonable to believe that ion/molecule reactions happening in a real sample should also be favored by the same conditions. However, there is the possibility that ions formed in the bulk could be reneutralized on their way to the vacuum.

3.3. Experimental Observations. It can be shown that the isolation of large analyte molecules by the matrix is actually a prerequisite to their emission as intact species in some cases. This effect is illustrated in Figure 12. In this case, a toluene solution containing oligomers of poly(4-methylstyrene) (P4MS: $M_n = 3930$ Da) and tetraphenylnaphthalene (TPN: MW = 432 Da) has been prepared with a weight ratio of 1 mg of analyte per 10 mg of matrix.[49] For comparison, another toluene solution has been made with 10 mg of poly(4-methylstyrene) and no TPN matrix. Both solutions were cast onto silicon wafers. Afterward, Au atoms were evaporated on both samples (20 nmoles/cm^2) to provide an external ionizing agent. With these materials and procedures, described in detail in ref 49, the desorption and ionization stages of the interaction are decoupled. Indeed, the ionization efficiency is related to the gold coverage and should not be influenced by the matrix whose chemical nature resembles that of the analyte.

Several regions of the positive mass spectrum of the pure P4MS sample are shown in Figure 12a. The fingerprint spectrum (inset 1) reveals the characteristic peaks of P4MS ($C_8H_9^+$; $C_7H_7^+$) and compares well with the mass spectra provided by the literature,[73] demonstrating the presence of a P4MS film on the surface. In the high-mass range, however, one notices only a few relatively weak peaks corresponding to gold clusters but no P4MS molecular ions. Finally, the region encompassing the mass range of 300−600 Da (inset 2) confirms the expected absence of TPN molecules. For comparison, the high-mass range corresponding to the mixed TPN/P4MS film is shown in Figure 12b. In this case, the Au-cationized P4MS molecules constitute a relatively intense distribution of peaks, consistent with the experimental distribution of molecular weights of the sample even though the absolute quantity of P4MS is 10 times lower in the matrix-containing sample. The inset shows intense peaks corresponding to the TPN molecule (432 Da) and its Au-cationized homologue (629 Da). Note that matrix−analyte clusters are not observed.

In contrast, our recent results also show that *shorter* PS oligomers (2 kDa) can be readily emitted from either pure PS films or TPN/PS mixtures.[49] Considering this broader perspective, the results with P4MS analytes confirm that isolation by the matrix helps disentangle large PS molecules (beyond 3000 Da) so that they can be sputtered intact. In addition, the absence of matrix−analyte clusters in the experiment depicted in Figure 12 is consistent with the fast unimolecular decomposition of homologue clusters predicted by the extended time simulations.

4. Conclusions and Perspective

From the fundamental viewpoint, our simulations show that the atomic collision cascade initiated by a 500-eV Ar projectile in the matrix/analyte organic medium is extinguished after a few hundred femtoseconds. A significant number of fragments and matrix molecules are directly ejected as a result of this collisional stage. Afterward, the remaining projectile energy is stored in the organic medium as vibrational excitation and molecular motion. Because molecular entities are weakly bound via van der Waals forces, the large organic clusters departing from the surface tend to break apart, releasing together buried analyte molecules and a "second batch" of matrix molecules that exhibit similar velocities. On a much smaller scale, this stage of the sputtering process is reminiscent of the collective motions observed in laser ablation, and the observed velocities are comparable.

The MD model predicts and explains a number of practical observations, and it supports several theoretical concepts previ-

ously derived from the experiments. These points of convergence and the developments they suggest are summarized hereafter.

Embedding a 2-kDa PS molecule in a low molecular weight matrix or depositing the same molecule on a silver substrate give rise to desorption yields of the same order of magnitude. This result is consistent with the experimental observation that parent ions of molecules of this size can be sputtered almost as efficiently from thick layers and submonolayers on metals, provided that an ionizing agent is present in both cases.[49] For such molecules, we believe that the matrix enhancement claimed by several authors[6,8,10] must be attributed almost exclusively to ionization effects. Additionally, for *larger* analyte molecules, the isolation provided by the matrix helps disentangle polymeric chains, thereby permitting their ejection as intact molecules from a thick layer. The two recognized effects of the matrix, namely, the isolation of the analyte molecules and their ionization, can be decoupled by using a chemically inert matrix in combination with an external ionizing agent (evaporated metal atoms,[49] noble or alkali metal salts).

Confining the organic sample in a "nanostructured" inorganic crystal improves the sputtering yields by a factor of 2. This enhancement is almost independent of the crystal atom mass. It is an effect of the weak energy coupling between the organic medium and the crystalline substrate, causing an enhanced reflection of the momentum toward the vacuum. This result is strongly reminiscent of the DIOS (desorption/ionization on porous silicon) enhancement effect observed in the laser ablation of organic materials adsorbed on porous silicon.[74,75] The physical explanation is probably related because the momentum is already distributed into vibrational excitation and molecular motion modes (rather than the SIMS/MALDI specific energy-transfer modes) when energy reflection by the substrate occurs. Porous inorganic substrates should also provide an enhancement of the sputtering yield in SIMS.

Conversely, the specific energy-transfer step and interaction volume of SIMS should be taken into account to develop novel matrices or matrix structures that are no longer derived from MALDI procedures,[6,8−10] where the photon absorption physics is crucial. Among the new sample (nano)structures, the use of a primer molecular layer as a substrate/matrix for analyte characterization (cocaine hydrochloride,[7] self-assembled layers[11,12]) constitutes a conceptually interesting approach.

As proposed by Cooks et al.[21] and Michl,[36] departing analyte molecules are often solvated by a number of matrix molecules in our simulations. These clusters are metastable, and they decompose over the first hundred picoseconds. Therefore, they should not be observed in mass spectra collected after several tens of microseconds, in agreement with experimental results. However, such a fast decomposition process explains the observation of molecular ions being formed in the acceleration section of ToF spectrometers.[76]

The information depths calculated for atoms and fragments agree reasonably well with values that have been determined experimentally using silicon[77,78] and polymer substrates[79] covered by organic layers with different thicknesses. In particular, the reduction of the emission depth with increasing fragment size has been observed in the experiment.

Even though our model does not allow us to treat ion/molecule chemical reactions directly, the observation that H transfer reactions occur frequently in the energized medium supports the general belief that the enhanced ionization provided by the matrix occurs through proton transfer in the excited volume or in the expanding plume. Ongoing developments of the model include the implementation of selected ionization pathways in the MD algorithm to attain a more accurate description of the investigated systems and to predict secondary ion yields; this information is invaluable to SIMS analysts.

Acknowledgment. A.D. acknowledges the Belgian Fonds National pour la Recherche Scientifique for financial support. Financial support from the National Science Foundation through the Chemistry Division is gratefully acknowledged by B.J.G. Additional computational resources were provided by the Center for Academic Computing of The Pennsylvania State University. We are also indebted to the Center for Academic Computing staff for their assistance with the Lion-xe cluster and for the development of new graphics software for animation and presentation.

References and Notes

(1) Garrison, B. J. In *ToF-SIMS: Surface Analysis by Mass Spectrometry;* Vickerman, J. C., Briggs, D., Eds.; SurfaceSpectra/IMPublications: Manchester, U.K., 2001; p 223.
(2) Garrison, B. J.; Delcorte, A.; Krantzman, K. D. *Acc. Chem. Res.* **2000**, *33*, 69.
(3) Krantzman, K. D.; Postawa, Z.; Garrison, B. J.; Winograd, N.; Stuart, S. J.; Harrison, J. A. *Nucl. Instrum. Methods Phys. Res., Sect. B* **2001**, *180*, 159.
(4) Delcorte, A.; Bertrand, P.; Garrison, B. J. *J. Phys. Chem. B* **2001**, *105*, 9474.
(5) Kerford, M.; Webb, R. P. *Nucl. Instrum. Methods Phys. Res., Sect. B* **2001**, *180*, 44.
(6) Wu, K. J.; Odom, R. W. *Anal. Chem.* **1996**, *68*, 873.
(7) Nicola, A. J.; Muddiman, D. C.; Hercules, D. M. *J. Am. Soc. Mass Spectrom.* **1996**, *7*, 467.
(8) Hanton, S. D.; Clark, P. A. C.; Owens, K. G. *J. Am. Soc. Mass Spectrom.* **1999**, *10*, 104.
(9) Szymczak, W.; Wolf, M.; Wittmaack, K. *Acta Hydrochim. Hydrobiol.* **2000**, *28*, 350.
(10) Wittmaak, K.; Szymczak, W.; Hoheisel, G.; Tuszynski, W. *J. Am. Soc. Mass Spectrom.* **2000**, *11*, 553.
(11) Van Stipdonk, M. J.; English, R. D.; Schweikert, E. A. *Anal. Chem.* **2000**, *72*, 2618.
(12) Michel, R.; Luginbuhl, R.; Graham, D. J.; Ratner, B. D. *Langmuir* **2000**, *16*, 6503.
(13) Fenselau, C. *Anal. Chem.* **1997**, *69*, 661A.
(14) Wu, K. J.; Odom, R. W. *Anal. Chem.* **1998**, *70*, 456A.
(15) Karas, M.; Bachmann, D.; Bahr, U.; Hillenkamp, F. *Int. J. Mass Spectrom. Ion Processes* **1988**, *78*, 53.
(16) Tanaka, K.; Waki, H.; Ido, Y.; Akita, S.; Yoshida, Y.; Yoshida, T. *Rapid Commun. Mass Spectrom.* **1988**, *2*, 151.
(17) Jonkman, H. T.; Michl, J.; King, R. N.; Andrade, J. D. *Anal. Chem.* **1978**, *50*, 2078.
(18) Liu, L. K.; Busch, K. L.; Cooks, R. G. *Anal. Chem.* **1981**, *53*, 109.
(19) Busch, K. L.; Hsu; B.-H.; Xie, Y.-X.; Cooks, R.-G. *Anal. Chem.* **1983**, *55*, 1157.
(20) Busch, K. L.; Hsu, B. H.; Xie Y.-X.; Cooks, R. G. In *Ion Formation from Organic Solids (IFOS II);* Benninghoven, A., Ed.; Springer-Verlag: Berlin, 1983; p 138.
(21) Cooks, R. G.; Busch, K. L. *Int. J. Mass Spectrom. Ion Phys.* **1983**, *53*, 111.
(22) Ross, M. M.; Colton, R. J. *Anal. Chem.* **1983**, *55*, 50.
(23) Ross, M. M.; Colton, R. J. *J. Vac. Sci. Technol., A* **1983**, *1*, 441.
(24) Busch, K. L.; Unger, S. E.; Cooks, R. G. In *Ion Formation from Organic Solids (IFOS I);* Benninghoven, A., Ed.; Springer-Verlag: Berlin, 1981.
(25) Surman, D. J.; Vickerman, J. C. *J. Chem. Res., Synop.* **1981**, *170*.
(26) Barber, M.; Bordoli, R. S.; Sedgwick, R. D.; Taylor, A. N. *J. Chem. Soc., Chem. Commun.* **1981**, 325.
(27) Barber, M.; Bordoli, R. S.; Elliot, G. J.; Sedgwick, R. D.; Taylor, A. N. *Anal. Chem.* **1982**, *54*, 645A.
(28) Williams, P.; Gillen, G. In *Ion Formation from Organic Solids (IFOS IV);* Benninghoven, A., Ed.; Wiley & Sons: Chichester, U.K., 1988; p 15.
(29) Gillen, G.; Christiansen, J. W.; Tsong, I. S. T.; Kumball, B.; Williams, P. *Rapid Commun. Mass Spectrom.* **1988**, *2*, 67.
(30) Bennett, J.; Gillen, G. *J. Am. Soc. Mass Spectrom.* **1993**, *4*, 930.
(31) Gillen, G.; Hues, S. M. *J. Am. Soc. Mass Spectrom.* **1993**, *4*, 419.

(32) Szymczak, W.; Wittmaack, K. *Rapid Commun. Mass Spectrom.* **2002**, *16*, 2025.
(33) Pachuta, S. J.; Cooks, R. G. *Chem. Rev.* **1987**, *87*, 647.
(34) Itina, T. E.; Zhigilei, L. V.; Garrison, B. J. *J. Phys. Chem. B* **2002**, *106*, 303.
(35) Zhigilei, L. V.; Yingling, Y. G.; Itina, T. E.; Schoolcraft, T. A.; Garrison, B. J. *Int. J. Mass Spectrom.* (Franz Hillenkamp special issue), in press.
(36) Michl, J. *Int. J. Mass Spectrom. Ion Phys.* **1983**, *53*, 255.
(37) Shiea, J.; Sunner, J. In *Methods and Mechanisms for Producing Ions from Large Molecules;* Standing, K. G., Ens, W., Eds.; Plenum Press: New York, 1991.
(38) Wong, S. S.; Röllgen, F. W. *Nucl. Instrum. Methods Phys. Res., Sect. B* **1986**, *436*, 447.
(39) Colton, R. J.; Campana, J. E.; Kidwell, D. A.; Ross, M. M.; Wyatt, J. R. *Appl. Surf. Sci.* **1985**, *21*, 168.
(40) Stuart, S. J.; Tutein, A. B.; Harrison, J. A. *J. Chem. Phys.* **2000**, *112*, 6472.
(41) Delcorte, A.; Garrison, B. J. *J. Phys. Chem. B* **2000**, *104*, 6785.
(42) Chatterjee, R.; Postawa, Z.; Winograd, N.; Garrison, B. J. *J. Phys. Chem. B* **1999**, *103*, 151.
(43) Delcorte, A.; Vanden Eynde, X.; Bertrand, P.; Vickerman, J. C.; Garrison, B. J. *J. Phys. Chem. B* **2000**, *104*, 2673.
(44) Moon, D. W.; Winograd, N.; Garrison, B. J. *Chem. Phys. Lett.* **1985**, *114*, 237.
(45) Taylor, R. S.; Garrison, B. J. *Langmuir* **1995**, *11*, 1220.
(46) Liu, K. S. S.; Yong, C. W.; Garrison, B. J.; Vickerman, J. C. *J. Phys. Chem. B* **1999**, *103*, 3195.
(47) Delcorte, A.; Arezki, B.; Bertrand, P.; Garrison, B. J. *Nucl. Instrum. Methods Phys. Res., Sect. B* **2002**, *193*, 768.
(48) Delcorte, A.; Bertrand, P.; Garrison, B. J. *Appl. Surf. Sci.* **2003**, *166*, 203.
(49) Delcorte, A.; Médard, N.; Bertrand, P. *Anal. Chem.* **2002**, *74*, 4955.
(50) Harrison, D. E., Jr. *Crit. Rev. Solid State Mater. Sci.* **1988**, *14*, S1.
(51) Winograd, N.; Garrison, B. J. In *Ion Spectroscopies for Surface Analysis*; Czanderna, A. W., Hercules, D. M., Eds.; Plenum Press: New York, 1991; p 45.
(52) Brenner, D. W. *Phys. Rev. B* **1990**, *42*, 9458.
(53) Brenner, D. W.; Harrison, J. A.; White, C. T.; Colton, R. J. *Thin Solid Films* **1991**, *206*, 220.
(54) Brenner, D. W.; Shenderova, O. A.; Harrison, J. A.; Stuart, S. J.; Ni, B.; Sinnott, S. B. *J. Phys.: Condens. Matter*, in press.
(55) Anderson, A. B.; McDevitt, M. R.; Urbach, F. L. *Surf. Sci.* **1984**, *146*, 80.
(56) Dudde, R.; Frank, K. H.; Koch, E. E. *Surf. Sci.* **1990**, *225*, 267.
(57) Stave, M. S.; Sanders, D. E.; Raeker, T. J.; DePristo, A. E. *J. Chem. Phys.* **1990**, *93*, 4413.
(58) Garrison, B. J. *Chem. Soc. Rev.* **1992**, *21*, 155.
(59) Harrison, D. E., Jr.; Delaplain, C. B. *J. Appl. Phys.* **1976**, *47*, 2252.
(60) Wucher, A.; Garrison, B. J. *Phys. Rev. B* **1992**, *46*, 4855.
(61) Schoolcraft, T. A.; Constable, G. S.; Jackson, B.; Zhigilei, L. V.; Garrison, B. J. *Nucl. Instrum. Methods Phys. Res., Sect. B* **2001**, *180*, 245.
(62) Itina, T. E.; Zhigilei, L. V.; Garrison, B. J. *Nucl. Instrum. Methods Phys. Res., Sect. B* **2001**, *180*, 238.
(63) Williams, P.; Sundqvist, B. U. R. *Phys. Rev. Lett.* **1987**, *58*, 1031.
(64) Hillenkamp, F.; Karas, M.; Bahr, U.; Ingendoh, A. In *Ion Formation from Organic Solids (IFOS V);* Hedin, A., Sundqvist, B. U. R., Benninghoven, A., Eds.; Wiley: Chichester, U.K., 1990; p 111.
(65) Taylor, R. S.; Brummel, C. L.; Winograd, N.; Garrison, B.; Vickerman, J. C. *Chem. Phys. Lett.* **1995**, *233*, 575.
(66) Taylor, R. S.; Garrison, B. J. *Int. J. Mass Spectrom. Ion Processes* **1995**, *143*, 225.
(67) Beardmore, K.; Smith, R. *Nucl. Instrum. Methods Phys. Res., Sect. B* **1995**, *102*, 223.
(68) Zhigilei, L. V.; Kodali, P. B. S.; Garrison, B. J. *J. Phys. Chem. B* **1998**, *102*, 2845.
(69) Huth-Fehre, T.; Becker C. H. *Rapid Commun. Mass Spectrom.* **1991**, *5*, 378.
(70) Marletta, G.; Catalono, S. M.; Pignataro, S. *Surf. Interface Anal.* **1990**, *16*, 407.
(71) Sunner, J. *Org. Mass Spectrom.* **1993**, *28*, 805.
(72) Taylor, R. S.; Garrison, B. J. *J. Am. Chem. Soc.* **1994**, *116*, 4465.
(73) *The Static SIMS Library*; Vickerman, J. C., Briggs, D., Henderson, A., Eds.; SurfaceSpectra: Manchester, U.K., 1997.
(74) Wei, J.; Buriak, J.; Siudzak, G. *Nature (London)* **1999**, *401*, 243.
(75) Shen, Z.; Thomas, J. J.; Averbuj, C.; Broo, K. M.; Engelhard, M.; Crowell, J. E.; Finn, M. G.; Siudzak, G. *Anal. Chem.* **2001**, *73*, 612.
(76) Delcorte, A.; Bertrand, P. *Surf. Sci.* **1998**, *412/413*, 97.
(77) Delcorte, A.; Bertrand, P.; Arys, X.; Jonas, A.; Wischerhoff, E.; Mayer, B.; Laschewsky, A. *Surf. Sci.* **1996**, *366*, 149.
(78) Delcorte, A. In *ToF-SIMS: Surface Analysis by Mass Spectrometry*; Vickerman, J. C., Briggs, D., Eds.; SurfaceSpectra/IM Publications: Manchester, U.K., 2001; p 161.
(79) Delcorte, A.; Bertrand, P.; Wischerhoff, E.; Laschewsky, A. *Langmuir* **1997**, *13*, 5125.